Overcoming thermal degradation during continuous conversion of water into hydrogen peroxide in a flexible plasma reactor

Mery S. Hernandez[*], Yannis Mikolaiczyk[*], Sergey Soldatov[~], Guido Link[~], Lucas Silberer[~], Roland Dittmeyer[*], Alexander Navarrete*

*Institute for Micro Process Engineering, Karlsruhe Institute of Technology, Karlsruhe, 76344, Germany

~Institute for Pulsed Power and Microwave Technology, Karlsruhe Institute of Technology, Karlsruhe, 76344, Germany

Supporting Information Placeholder

ABSTRACT: By control of the nanosecond pulsation, energy input and flow it is possible to achieve commercial-level hydrogen peroxide (H_2O_2) concentrations using only water and plasma in a continuous process while minimizing thermal degradation. Time-resolved ultrafast Optical Emission Spectroscopy was employed to observe the formation of reactive species, shedding light on the underlying mechanisms. This study also highlights the critical role of thermal degradation, which was effectively managed through quenching of the plasma zone. A parametric scan of pulse duration and pulse repetition frequency of the microwave power showed a significant influence on the H_2O_2 formation, whereby the mean power also plays an important role. Additionally, H_2O_2 concentration was found to be inversely proportional to the water flow rate. A maximum concentration of 0.17 wt% was achieved with 1.2 g/kWh based on the absorbed power at a flow rate of 0.2 mL/min. This plasma reactor technology shows promise for further development as a decentralized solution for green chemical synthesis of H_2O_2.

Introduction

The demand for hydrogen peroxide (HP), a versatile and environmentally friendly oxidant, is rapidly increasing (4% per year). (1–3) It is valued for its green properties as it decomposes only into H_2O and O_2. Nevertheless, its traditional synthesis method, the anthraquinone oxidation process (AOP), has significant drawbacks, including high carbon emissions, substantial waste generation, and challenges in transportation. (4,5) Such challenges are further related to the temperature-sensitive nature of HP. A promising solution is the decentralized, on-site synthesis of HP using renewable energy. This approach not only reduces the environmental impact of HP synthesis but also supports the transition to renewable energy in the economy. (6) Thus, as sustainability becomes a global priority, interest in greener alternatives for HP production continues to grow. (7,8) Several approaches have been explored as potential, sustainable options to the conventional AOP, including direct synthesis, photocatalysis, electrolysis, and plasma-based methods. (9–11) Plasma technology potential lies on its rapid reaction rates, critical-materials-free operation, and compatibility with intermittent renewable energy sources, making them ideal for decentralized, on-site HP production. (12,13) High temperatures are detrimental for HP synthesis, (14,15) therefore, non-equilibrium cold plasma configurations (e.g. DBD) favouring lower temperatures have traditionally been used to increase the yield of HP. (13,16–23) Microwave plasmas are not usually employed for hydrogen peroxide synthesis, mainly due to the high temperatures they can achieve (~5 - 8 x10^3 K).(24) Yet, in terms of efficiency, microwave (MW), warm plasmas have demonstrated high performance in other processes in which reaching high temperatures is not an issue. (25,26) At the same time, for the plasma based synthesis of HP it is necessary to first dissociate the water molecules and create OH radicals, which is favored by high temperatures (Figure S1). According to literature, these radicals can then recombine to form HP. (27–29) This last stage is a three-body reaction that is favoured at lower temperatures due to increased collision efficiency.(30–33)
Looking to create a decentralized solution we propose and demonstrate, for the first time, the use of a plasma reactor that makes use of nanosecond microwave pulsation to promote quenching of the plasma during continuous HP synthesis. (34,35) The quenching promoted by ultrafast pulsation is complemented with the discharge contacting a cold surface provided by a heat exchanger (Figure 1a). Our results show near-commercial concentrations of HP directly from water, without the use of catalysts nor additional additive into the water, using a compact and tuneable reaction system (Figure 1b).

Results and discussion

The integration of the nanosecond-pulsed microwave plasma system with a cooling loop (using liquid water at 18°C) (Figure S2) for enhanced quenching resulted in higher hydrogen peroxide (HP) recoveries (more details in Figure S3). This finding suggests that maintaining lower temperatures within the plasma-liquid interface zone is crucial for optimizing the HP formation pathways and ensuring its further stabilization. For a broad understanding of the microwave plasma system that we present here, a series of parametric studies were carried out with the plasma quenching included, and the investigated HP concentration was followed by UV-Vis spectroscopy (more details in Supporting Information-Section 1).

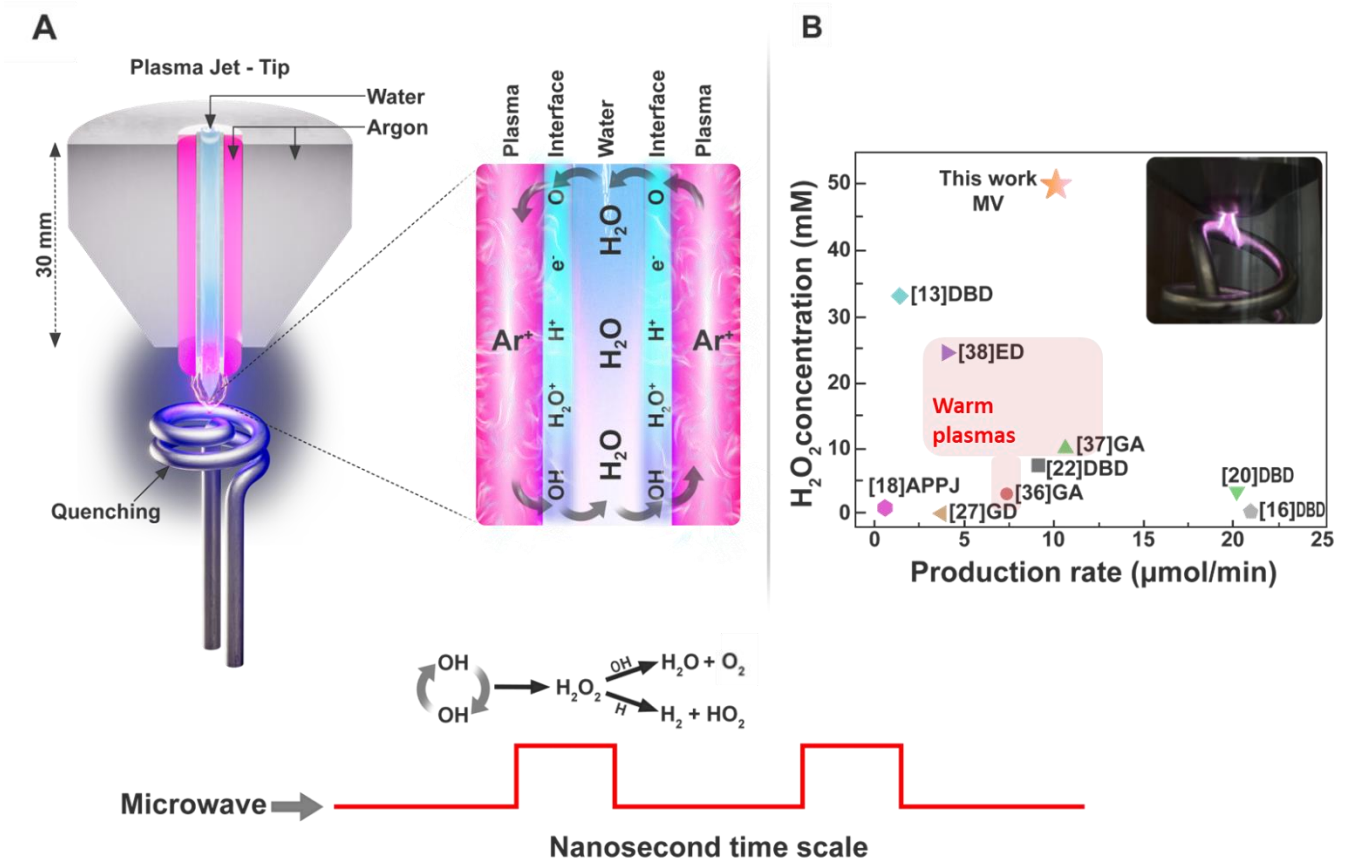

Figure 1. Nanosecond pulsed microwave plasma-based synthesis of H_2O_2 integrated with plasma quenching. (A) Schematics of the plasma at the tip of the reactor and quenching system. (B) Comparison of maximum H_2O_2 concentration achieved by this work and different plasma-based methods: Dielectric Barrier Discharge (DBD) using He+H_2O, (13) DBD using Ar+H_2O vapor, (16) Atmospheric Pressure Plasma Jet (APPJ) using He+H_2O(18), DBD using NaCl solution added to H_2O, (20) DBD using H_2O steam, (22) Glow Discharge (GD) using He+H_2O (27), Gliding Arc (GA) using Ar + H_2O, (36) GA using Ar+H_2O spray, (37) Electrical Discharge (ED) using Ar+H_2O, (38) and this work with Microwaves (MW) and Ar+H_2O at the highest HP concentration achieved within the study.

The duration of microwave pulses (pulse-time or "t_on") was varied within 100 ns and 10 μs, and the peak power was varied within 300 and 900 W. The duty cycle (DC) was calculated as the fraction of t_on over the period of pulsation (t_on+t_off), more details in Supporting Information-Figure S4. The results of a scan of peak power along with pulse time at a fixed duty cycle of 0.3, and 2.5 mL/min of water flow are presented in Figure 2a. At these conditions the maximum and minimum HP concentrations were observed between 500 ns and 1000 ns of t_on, for all tested peak power values. Specifically, at 700 ns of t_on, corresponding to a pulsation frequency of 0.4 MHz (calculated as DC/t_on), the impact of peak power on HP concentration was more clear as compared to 500 ns or 1000 ns of t_on. At this specific pulse time (700 ns t_on), HP concentrations peaked at 6.5 mM and dropped to as low as 0.5 mM, along peak power increase.

The results indicate that at a pulse duration of 700 ns, the relationship between peak power and H_2O_2 concentration becomes more predictable, leaving the possibility to optimize the power input for improving the hydrogen peroxide production at the plasma–water interface. This observation may be linked to the lifetime of short-lived reactive species involved in HP formation. For instance, the OH radical in its excited state, OH(A), has a lifetime of approximately 700 ns. (21,39) Furthermore, for longer t_on values of 5 and 10 μs (see insertion in Fig.2a), concentrations lower than 3 mM were observed, with minimal variation across different input powers. This suggests that prolonged pulse times may hinder the HP generation, probably due to the extended exposure of the active species (i.e. OH) to elevated gas temperatures, which could lead to HP degradation after its formation. (40) As observed by Lietz et al. if the conversion of H_2O into H_2O_2 (via electron impact dissociation to produce OH, followed by OH + OH + M → H_2O_2 + M) takes longer than the pulsation period, there would be an accumulation of OH from pulse to pulse, which could easily lead to H_2O formation, or HP consumption via OH + H_2O_2 → H_2O + O_2^-. (40)

The average HP production rate ranged from 0.01 to 0.26 μmol/s and variated proportionally with concentration, as the water flow was kept constant. In terms of energy yield (Figure S5), values reached up to 0.25 g/kWh in average, affected mainly by the t_on variation. One of our findings is that the use of continuous microwave power resulted only in low HP concentrations, with a negligible variation along power input (Fig. S5 -line "cw"). Such finding supports the hypothesis that continuous microwave tends to

generate warm plasmas, which negatively impact the HP production.

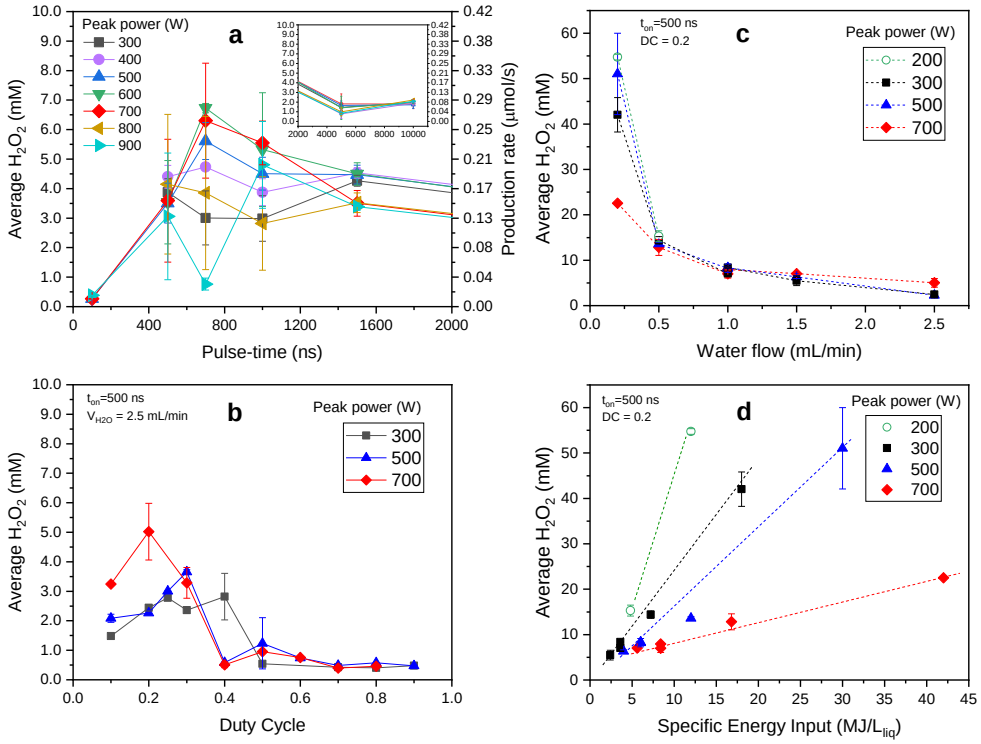

Figure 2. Experimental characterization of the system for HP concentration in function of: (A) Pulse-time, (B) Duty cycle, (C) water flow rate, and (D) specific energy input, for different input power values. For figure (a), a constant water flow of 2.5 mL/min and 0.3 of duty cycle were used. The duty cycle scan (b) is presented for 500 ns pulse-time, 2.5 mL/min of water. The water flow rate (c) and Specific energy input per liquid flow (MJ/L liquid) (d) scans were taken at 0.2 DC and 500 ns of pulse-time. The error bars in the graphics include three replicates. All experiments used 8.7 L/min of argon.

Consequently, this reinforces the importance of using nanosecond pulsed microwaves to achieve lower gas temperatures, hence increasing the HP production, given that HP can be stabilize in the products of water dissociation at low temperatures.(30)

By scanning peak-power, we observed that it significantly affects the HP production, depending on the pulse duration. To explore this further, we chose three peak power settings that would give us an overview of the power effect: 300 W (low), 500 W (medium), and 700 W (high). We then proceeded to study the DC variation in steps of 0.1, from 0.1 up to 0.9. Varying the DC directly affects the mean power coupled into the plasma reaction zone (peak power*DC ≈ mean power). In this sense, higher duty cycles — which correspond to higher mean power — will result in higher HP production for the same peak power. In fact, Du et al. reported that both OH and HP densities increased significantly with mean power input, with a factor of 2 times higher for argon than for helium gas, for a DBD plasma reactor at atmospheric pressure. (16) Vasko et al., also reported a similar trend where higher duty cycles at a fixed peak power increased the concentration of HP in an atmospheric pressure glow discharge reactor. (27) Moreover, Soldatov et al. for CO_2 splitting in atmospheric microwave plasma, and fixed peak power of 220 W has found that the CO_2 conversion increased with the DC, for different tested pulse duration. (34) Wandell et al. observed a similar effect by studying HP production in a pulsed water spray plasma reactor using gliding arc: the production rate increased with the mean discharge power. (36) However, a slight opposite trend was observed in the present work: lower concentrations were achieved along increasing DC beyond 0.4, for every tested peak power (Figure 2b). Although increasing the duty cycle appeared to reduce HP production, it is noteworthy that the highest HP concentration was achieved at the highest tested peak power of 700 W — but at the lowest duty cycle of 0.2. In other words, at a pulse duration of 500 ns, a DC of 0.2 favours HP formation under higher peak power conditions. The latter conditions correspond to a mean power of ~140 W delivered in 500 ns bursts at a pulsation frequency of 0.4 MHz —remarkably, the same frequency at which a maximum concentration was previously found under a fixed DC of 0.3 (Fig. 2a). This suggests that optimum H_2O_2 concentrations can be achieved using different microwave parameter combinations, particularly around a pulsation frequency of 0.4 MHz.

Additionally, the DC scan at different peak power inputs revealed multiple H_2O_2 concentration peaks. For instance, a second peak was found for a DC of 0.4 at 300 W (Fig. 2b), corresponding to 0.8 MHz and 120 W of mean power; while the other peak power inputs (500W and 700 W) revealed rather high loss of HP at such DC. Increasing the DC beyond 0.4 (Fq > 0.8 MHz) resulted in a decrease of HP concentration, and for DC values between 0.7 and 0.9, variations in peak power had minimal effect. The latter observation could be related to an excess of thermal energy, which could negatively affect the formation reaction of HP and its recovery from the plasma-water interface. Furthermore, the impact of the

pulse duration was found to be less significant than that of the DC in determining H_2O_2 concentration (Figure S6).

Notably, after analysing the DC variation across different peak power inputs, the earlier observation of an optimum pulsation frequency around 0.4 MHz remains consistent. However, this optimum may shift under different water flow conditions. To explore this possibility, we next investigated the effect of varying water flow rates at a DC of 0.2, which previously yielded the highest HP concentration. We selected similar peak power values as in the earlier tests (200 W, 300 W, 500 W and 700 W), and the results are presented in Figure 2c. In general, decreasing the water flow rate had a positive effect over the HP concentration, with a maximum average HP of ca. 50 mM for 0.2 mL/min of water flow. This can be related to the increase of residence time at lower water flow rates allowing longer treatment of the water under pulsed plasma discharge. At 500 ns of pulse time and DC of 0.2, the residence time of water in the plasma zone went from 508 ms (at 2.5 mL/min of water) to 6.36 s (at 0.2 mL/min of water), receiving ca. $2.5x10^6$ pulses of plasma in the latter case (more details in Supplementary information-Section 1). In the specific case of 0.2 mL/min of water flow, there was a clear difference between peak power variations, and the highest concentration was achieved at the lowest peak power applied of 200 W, while increasing the power resulted in decreased HP concentration. On the other hand, when examining H_2O_2 concentration as a function of water flow rate, each tested power input exhibited a consistent trend: the concentration decreased following a negative exponential relationship (Figure 2c). Such a trend appeared to be independent on both pulse-time (t_on) or DC variations (Figure S7a-b). A similar behavior was reported by Cameli et al., who studied the effect of varying liquid flow rates in a helical coaxial DBD plasma reactor. They found that H_2O_2 concentration decreased with increasing water flow rate, reaching a maximum of 33 mM at the lowest tested flow of 0.05 mL/min. The authors attributed this behavior to changes in the gas-to-liquid ratio, which influence droplet formation and the interfacial area available for plasma–liquid interaction. (13) Such explanation could also be applied in our case, given that, at a constant gas flow rate, lowering the water flow rate would only increase the residence time of the water, and allow a longer exposition of water droplets to the plasma phase. Nevertheless, this does not explain why at 0.2 mL/min of water, the maximum concentration was achieved at the minimum power input.

Looking at the specific energy input variation in function of the water flow rate (SEI_L), one can also have an additional parameter to analyze the plasma-liquid interaction. In our case, SEI_L variations between 5 to 44 MJ/L were observed for the different power inputs (Figure 2d). In general, higher SEI_L values (lower water flow rates) led to higher HP concentrations at a fixed peak power, pulse time and DC, following a quasi linear trend represented by the dashed line Figure 2d. The production rate ranged between 0.08 and 0.22 µmol/s, following apparent trends in which lower SEI_L values were associated with higher production rates (Figure S7c-f). The average energy yield (g/kWh) (calculated with theoretical mean power) was found within a range of 0.01 – 0.6 g/kWh, as presented in Figure 3. It is evident that some specific points present a higher performance (Hp concentrations > 20 mM), as marked in the highlighted zone in the figure. These points belong to a water flow rate of 0.2 mL/min, which as discusses before, led to the highest concentrations achieved here. Even though the trend is not linear, it is possible to tune the system aiming for higher energy yields without sacrificing the HP concentration (more details in Figure S8). Nevertheless, after measuring the effective absorbed power (based on microwave energy absorbed by the plasma), we found that the energy yield was higher, reaching up to 1.2 g/kWh when yielding the highest HP concentration (more details in Figure S9). The analysis of the energy usage and energy yield showed that a modification of the applied microwave power must be implemented to avoid high energy losses and increase energetic efficiency. The gas to liquid ratio was also analyzed for gas flow rates between 4 - 10 L/min, and liquid flow rates of 0.2 – 5 mL/min. In general, higher HP concentrations were found at larger gas to liquid ratios (>40 $x10^3$) within the studied ranges (more details in Figure S10).

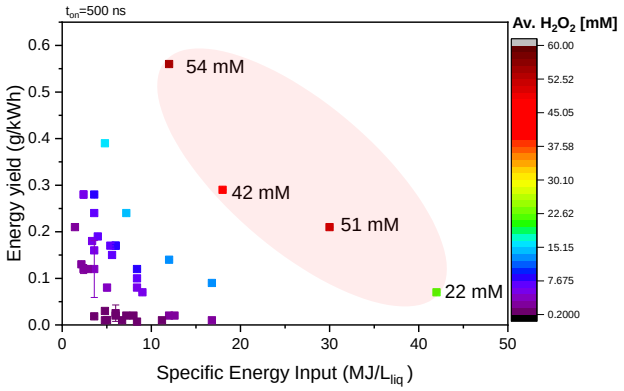

Figure 3. Energy yield versus specific energy input at different HP concentrations. The results varying the water flow rate between 0.2 and 2.5 mL/min, the peak power between 200 W and 700 W, and the duty cycle between 0.1 and 0.7, at a fixed pulse time of 500 ns. The highlighted area in the graphic indicates the energy yield of the highest HP concentrations achieved while varying the specific energy input by adjusting the mean power at water flow rate of 0.2 mL/min.

The online use of Optical Emission Spectroscopy allows to gather an initial qualitative assessment of the reaction mechanisms. For the specific case of 0.2 mL/min of water flow at 0.2 DC (which led to the maximum HP concentrations here), a follow-up of the reactive species was obtained using a simple UV-Vis spectrometer, as described in the experimental setup in Supplementary Information - Section 1. The qualitative analysis is summarized in Figure 4, including temperature measurements of the gas near the plasma-water interaction zone (temperature of reaction environment), for tests without and with quenching. All intensities were normalized to the H_α spectral line. The behaviour of the reactive species was evidently different for the experiments without quenching compared to those ones with quenching. In general, the presence of OH (309 nm), H_α (656 nm), H_β (485 nm), O (777 and 844 nm) and Ar lines were predominant.

Before explaining the variation of the observed active species, and the possible reaction mechanism, we can consider that the very first steps during plasma-water interaction are the water splitting and OH formation. The main reactions associated to the formation of OH (A-X) radicals via the dissociation of water molecules in argon plasma are electron impact dissociation (Eq. 1), electron-ion

dissociative recombination (Eq. 2), dissociation by metastable species of argon (Eq. 3), Penning ionization for H_2O^+ production (Eq. 4), and thermal dissociation (Eq. 5) which occurs at elevated temperatures around 3500 – 4000 K, as reported before. (11,21,29,41)

$$e^- + H_2O \rightarrow OH + H + e^- \quad \text{Eq. 1}$$
$$e^- + H_2O^+ \rightarrow OH + H \quad \text{Eq. 2}$$
$$Ar^+ + H_2O \rightarrow OH + H + Ar \quad \text{Eq. 3}$$
$$Ar^+ + H_2O \rightarrow e^- + H_2O^+ + Ar \quad \text{Eq. 4}$$
$$H_2O^* + H_2O \rightarrow OH + H + H_2O \quad \text{Eq. 5}$$

These reactions precede the formation of HP, due to ion recombination and interaction (Eq. 6-12): (17,29)

$$OH + OH \rightarrow H_2O_2 \quad \text{Eq. 6}$$
$$HO_2 + HO_2 \rightarrow H_2O_2 + O_2 \quad \text{Eq. 7}$$
$$HO_2^- + H^+ \rightarrow H_2O_2 \quad \text{Eq. 8}$$
$$H_3O^+ + HO_2^- \rightarrow H_2O_2 + H_2O \quad \text{Eq. 9}$$
$$HO_2^- + H_2O \rightarrow H_2O_2 + OH^- \quad \text{Eq. 10}$$
$$OH + H_2O^* \rightarrow H_2O_2 + H \quad \text{Eq. 11}$$
$$H_2O + H_2O \rightarrow H_2 + H_2O_2 \quad \text{Eq. 12}$$

The formation of the HO_2 and hydrated ion H_3O species, may originate from the following step reactions: (11,29)

$$2H_2O \rightarrow OH^- + H_3O^+ \quad \text{Eq. 13}$$
$$OH + O^- \rightarrow HO_2^- \quad \text{Eq. 14}$$
$$H_2O^+ \rightarrow OH + H_3O^+ \quad \text{Eq. 15}$$

Previous calculations from simulations have revealed that the OH radical species do no react with each other in the water phase. (42) i.e. Eq.6 takes place in the gas phase; however, the OH_2 radicals could react with each other in the water phase to form H_2O_2 and O_2 (Eq.7). (42) Nonetheless, the formation of HP can take place in the gas, the liquid, or at their interface. For the reaction at interface, the formed HP is then incorporated into the liquid. (43) In general, the mechanisms occurring at the gas-liquid interface are not completely clear yet. It has been stated before that such reactions are dependent on the temperature conditions, which affect the collisions, adsorption, and absorption phenomena happening in the interface. (20) High temperatures like those present in microwave plasmas are detrimental for the HP, (29) therefore not only the interaction of ions towards the formation of water (Eq. 16, 17) but also the HP decomposition (Eq. 18-20) due to thermal or radical or ion interactions need to be considered: (27)

$$OH + HO_2 \rightarrow H_2O + O_2 \quad \text{Eq. 16}$$
$$OH + OH^- \rightarrow H_2O + O^- \quad \text{Eq. 17}$$
$$OH + H_2O_2 \rightarrow H_2O + HO_2 \quad \text{Eq. 18}$$
$$H + H_2O_2 \rightarrow H_2 + HO_2 \quad \text{Eq. 19}$$
$$e + H_2O_2 \rightarrow OH^- + OH \quad \text{Eq. 20}$$

Having that in mind, we can observe that without plasma quenching (Figure 4a), the temperature rises along with microwave peak power, leading to a decrease of the HP concentration despite the observed presence of OH, H_β and O species. This suggests that not only the HP formation pathways are taking place, but also, and with more emphasis, the HP decomposition pathways towards OH, O and H_2O formation, favoured by a raise in temperature, as represented in equations 16 to 20.

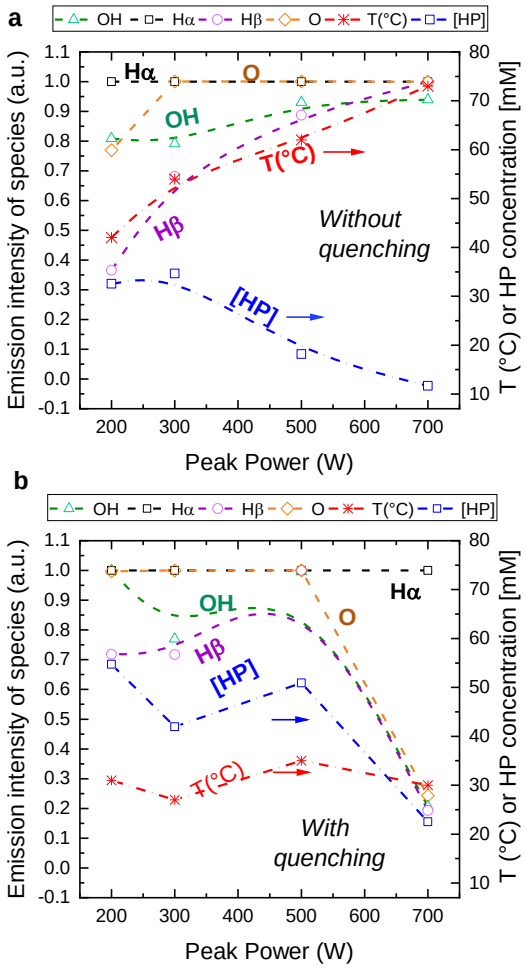

Figure 4. Qualitative spectral analysis of the emission intensity of species, gas temperature near the reaction environment and HP concentration as a function of the peak power. (a) without quenching, (b) with quenching. The pulse time was fixed to 500 ns with a DC of 0.2 and 0.2 mL/min of water. Dashed lines included in the graphic for visual guidance. Intensities were normalized to the H_α peak.

Another interesting observation emerged during experiments with quenching, where the species H_β and OH appeared to behave as a monitor of the HP concentration (Figure 4b). For instance, at the maximum tested peak power of 700 W a significant decrease is observed in the H_β and OH emissions, as well as in the resulting HP concentration. It is interesting to note a possible link between the formation of HP and the availability of one specific type of hydrogen (H_β) and OH radicals, possibly following Eq. 11. In this sense, besides the recombination of OH, the interaction of H ions and HO_2 ions could also be considered for the HP production in this system (Eq. 8). (17)

The analysis of the gas composition could support the proposal of possible dominant species in the gas phase. Therefore, a mass balance was calculated, along with selectivities to H_2, O_2 and HP, as the reaction products -Tables S2 and S3. The analysis of the gas products revealed the presence of oxygen, hydrogen and steam, which can come from Eq. 7, 16 and 19, recombination reactions

(Eq. 21, 22) or due to water splitting (Eq. 23). (29,33) According to the gas composition, the process is more selective to H_2 than to O_2, possibly favouring the reaction in Eq. 19.

$$O + O \rightarrow O_2 \quad \text{Eq. 21}$$
$$H + H \rightarrow H_2 \quad \text{Eq. 22}$$
$$H_2O \rightarrow H_2 + 1/2O_2 \quad \text{Eq. 23}$$

With the information gathered so far, one can speculate about the possible reaction mechanisms and determining species interaction towards the formation of HP. However, a temperature analysis of the plasma would clarify whether a thermal process is more dominant in this case.

The gas temperature can be determined following the rotational temperature distribution (T_{rot}) of the OH (A-X) emission spectra.(44) Qazi et al., discussed the different temperatures in an electrical discharge generated plasma in contact with liquid, distinguishing between the gas and the liquid phase temperatures. (41) Nevertheless, if the rotational distribution does not follow a Boltzmann distribution, then T_{rot} cannot represent the gas temperature correctly, and this is commonly observed for non-equilibrium plasmas. (45) For instance, Bruggeman et al., studied a DC plasma discharge generated in water, investigating the discharge in the liquid mode and in the bubble mode. The authors reported OH rotational temperatures with non-Boltzmann distribution around 2950 K, revealing that the efficiency of HP formation is significantly smaller in the bubble mode than in the liquid mode. (46)

In this sense, the temperature in the plasma environment depends on the plasma system configuration. For an electrical discharge in water, a global reaction mechanism for HP formation has been discussed, as described by Eq. 24. (43)

$$6H_2O \rightarrow 4H_2 + O_2 + 2H_2O_2 \quad \text{Eq. 24}$$

Nevertheless, the plasma configuration and the way of contacting the plasma and the liquid medium highly affects the HP formation paths. In this work, we calculated the mass balance using the gas composition and liquid products, and for a specific set of experimental conditions, the following reaction coefficients were obtained:

$$27H_2O \rightarrow 26H_2 + 12.5O_2 + H_2O_2 \quad \text{Eq. 25}$$

The mass balance details are presented in the Supporting Information-Table S1. The main difference between Eq. 24 and 25 is the ratio between H_2O and H_2O_2, having a molar ratio from ~27:1 for the plasma configuration discussed here, and a molar ratio of ~ 27:26 between H_2O and H_2 (close to 1:1). The higher selectivity towards H_2 and O_2 formation rather than to H_2O_2 could be attributed to the dominance of OH-based reaction pathways to produce H_2O_2. As explained by Luo *et al*., the OH mainly produced by electron impact dissociation of water and hydration of H_2O^+ ($H_2O^+ + H_2O \rightarrow H_3O^+ + OH$) follows a destruction through a 3-body radical-radical recombination with water as the third body.

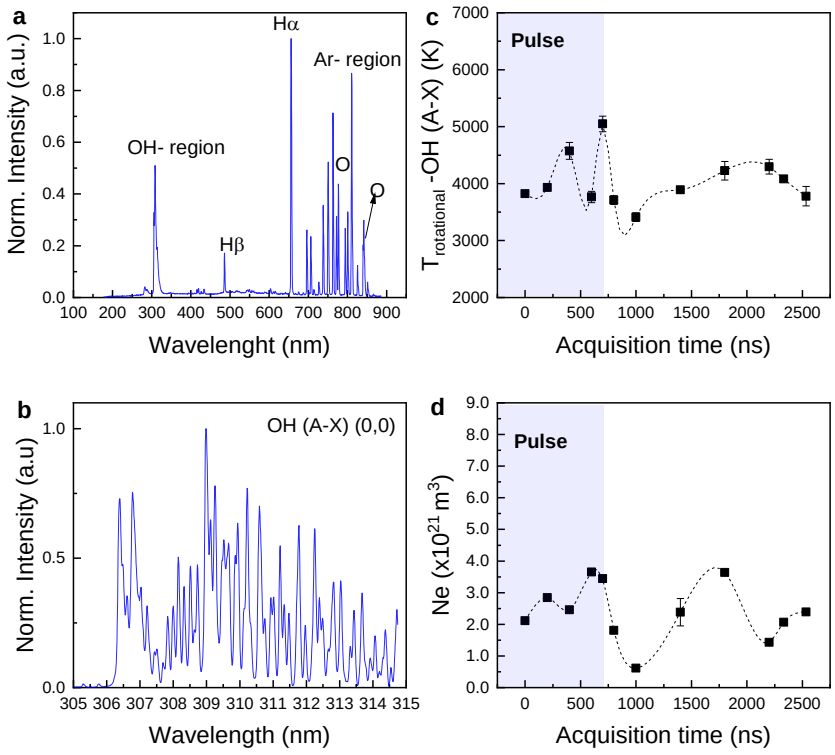

Figure 5. High resolution OES. (A) Low resolution overview OES spectrum, (B) High resolution OES spectrum with characteristic OH ro-vibrational emission bands, (C) OH rotational temperature versus acquisition time, and (D) electron density versus acquisition time. The spectra were taken for 2.5 mL/min of water, 8.7 L/min of argon, 500 W of peak power, pulse time of 700 ns and inter-pulse of 1633 ns (DC=0.3), with a total pulse period of 2333 ns. In figure 5b, the different lines indicate the OH transitions (A-X) for a representative acquisition time of 200 ns. The error bars represent the standard deviation from MassiveOES fitting.

In electronegative (low energy discharges) discharges, however, the recombination between positive ion (H_3O^+) and negative ions could significantly contribute to H formation, further leading to H_2 formation by interaction with water molecules.(47) If the production of H_2O_2 is dominated by radical recombination, the availability of energetic electrons becomes a key factor influencing the reaction pathway. In this context, electron density can serve as a guide for the energy available in the system. Low electron densities (i.e., low-energy discharges) tend to favor ion-neutralization reactions and H_2 formation, whereas high electron densities (or higher specific energy) promote OH radical generation through more frequent heavy-particle and electron-induced reactions, thereby enhancing H_2O_2 production.(47) Nevertheless, the destruction of H_2O_2 is also caused by OH, H and O species, or by the amount of vapor. Moreover, it has been reported that humidity can increase or decrease the formation of HP at certain energy input conditions. Gorbanev et al., reported that at elevated humidity (i.e. >60% in the gas feed) the HP in the liquid decreases. (44) In our case, we do not observe major influence of steam generation on the HP production rate. Nevertheless, we found that the system is more predictable at a DC of 0.2 while employing cooling (Figure S11). To further explain these phenomena, we analysed the temperature of the plasma zone following a high resolution (HR) time-resolved OES (Figure S12 presents the scheme of the configuration). The HR-OES results are summarized in Figure 5, including a representative spectrum acquired with a low resolution of 2 nm (Fig. 5a). The HR-OES for OH (A-X) ro-vibrational spectrum is presented in Figure 5b. With spectra fitting in MassiveOES we calculate the rotational temperature of OH species (OH-T_{rot}), and its variation along the pulse discharge is presented in Figure 5c. The spectra were recorded at different time delay between OES acquisition and beginning of microwave pulse. A full span of time delay was 2533 ns, which covers the total pulse period of 2333 ns. In this case, the OH-T_{rot} does not represent the gas temperature, given the non-equilibrium nature of this plasma configuration. Therefore, OH-T_{rot} (the temperature of the excited state) is used here as a guidance for possible reaction mechanisms.

The observed OH-T_{rot} were around 4000 K at the beginning of the pulse, which is higher than previous similar reports, indicating that the process starts following mainly a thermal dissociation. (29) The most prominent temperature (>5000 K) occurred at 700 ns, which is around the maximum life-time of the OH species. A decrease in temperature to below 3500 K was observed before 1000 ns, followed by a slight increase between 1400 ns and 2200 ns. Since the microwave pulse duration is 700 ns, this temperature evolution occurred during the inter-pulse period. This temporal evolution of OH rotational temperature could be linked to the complex interplay between radical formation mechanisms, internal energy transfer and relaxation processes involving different species. During the microwave pulse, the electron impact (Eq. 1, 2) and thermal dissociation (Eq. 4) reactions are the main mechanisms for formation of OH radicals. In this phase, the rotational energy is efficiently transported via vibrational-to-rotational (V-R) energy transfer, as energized electrons first excite vibrational modes, which subsequently relax into rotational excitation: $T_e \rightarrow T_{vib} \rightarrow T_{rot}$. (30) The efficiency and rate of V-R energy transfer vary depending on the collisional partners.

The observed increase in OH-T_{rot} during the inter-pulse phase (Fig. 5c) suggests that secondary excitation processes might be active. Given the relatively slow V–R relaxation of O_2 (100–1000 ns at 4000–5000 K, (48)) compared to faster species like H_2 [55], it is plausible that ion-molecule reactions involving O_2^+ and H_2O, such as $H_2O + O(^1D) \rightarrow 2OH$, (49) could lead to OH radicals carrying additional rotational energy, reflected as an increase in T_{rot}. However, this hypothesis requires further validation through time-resolved plasma diagnostics and kinetic modeling, and does not represent the focus of this study.

We can consider that the observed trend of the OH-T_{rot} is representative of the general process given that the residence time of the water in the plasma-water reaction zone, at these conditions of 2.5 mL/min and 700 ns of pulse time, would be 508 ms, and it is enough to receive 2.18 $x10^5$ cycles of pulses (more details in Supporting Information - Section 1). For the observed OH-T_{rot} values, the main OH formation pathway associated could fit to thermal dissociation (Eq. 5), which reported gas temperatures are between 2500 – 5000 K. (21)

Similar variations as in the OH-T_{rot} were also observed in the electron density (N_e) behavior (Figure 5d). N_e was estimated using the FWHM of the H_β line, as proposed in other studies. (46,50) This parameter can be calculated with both, H_β and H_α lines (Figure S13); nevertheless, H_β is preferred for small electron densities. (46) Our estimated N_e values, on the order of 10^{21} m^3, are in agreement with previous reports for similar plasma setups. (46) The variation of N_e along the pulse duration could be attributed to the interface dynamics (moisture, droplet generation, plasma liquid interaction, etc.). In this case, for both T_{rot} and N_e, a maximum around the same acquisition time (~700 ns) can be observed (Figure 5c-d), suggesting a correlation between high energy discharge and OH generation. It is interesting to observe that, at around this pulse time, higher H_2O_2 concentrations were found before (Fig. 1a), and could be related to heavy particles interaction dominating radical production, rather than leading to H and further H_2 formation.

Furthermore, the trend of N_e seems to decay over a period of 600 ns, between 800 and 1000 ns (Figure 5d), which is similar to the decay trend of T_{rot}, and raise again between 1000 ns and 1800 ns. As T_{rot} and N_e are calculated from OH and H_β, respectively, the fact that both trends follow a similar behavior in HR-OES supports the qualitative analysis previously discussed for OH and H_β species (Fig. 4b), where both species exhibited a similar trend to the H_2O_2 formation. Moreover, the evolution of T_{rot} and N_e in the inter-pulse time (after 700 ns, plasma off) could be related to longer living species (>1μs) like H_2, H_2O_2 and O_2, as observed by Luo et al.(47) The authors reported similar raising and decaying trends during the inter-pulse. Not stabilized H_2O_2 in the inter pulse time can act as an acceptor of hydrogen atoms and hydroxyl radical, leading to its thermal decomposition.(51) This reactions are exothermic and can contribute to an increase in temperature. Herin the importance of rapidly stabilize the formed H_2O_2 before its thermal decomposition happens, supporting the value of adding cooling to the plasma-water interaction zone. For instance, a positive effect of fast cooling of a nanosecond plasma was also reported by Chauvet et al. The authors claimed that cooling of the plasma -due to bubble expansion- reduces efficiency of second order reactions, for example instance, towards O_2 formation via OH dissociation into O and H,

which would participate in the decomposition of H_2O_2, as well as thermal degradation. (31)

In general, a thermal dissociation path for OH production appears to be more consistent with the observed rotational temperatures, followed by electron impact dissociation of water and further three-body radical recombination ($OH+OH+M \rightarrow H_2O_2+M$), enhanced at atmospheric pressure.(52) To develop a broader understanding of the plasma–water interface, we propose a global classification of the key reactions according to the phase in which they are likely to occur—namely, the gas phase, liquid phase, or the plasma–liquid interface.

Table 1. Categorization of key reactions in the plasma–liquid system

Plasma-liquid Interface	Ref.	*Rate constant k*
$H_2O + e^- \rightarrow OH + H + e^-$	(41)	$x10^{-18}$ (m^3s^{-1})
$H_2O + Ar^+ \rightarrow OH + H + Ar$	(21)	$x10^{-16}$ (m^3s^{-1})
$H_2O_{(l)} + H_2O^* \rightarrow OH + H + H_2O$	(21)	$x10^{-20}$ (m^3s^{-1})
$OH + H_2O^* \rightarrow H_2O_2 + H$	(29)	-
$H + H_2O^* \rightarrow H_2 + OH$	(30)	-
$H_2O^+ + H_2O \rightarrow OH^- + H_3O^+$	(11,21,40)	$x10^{-15}m^3s^{-1}$
Gas phase		
$HO_2 + H_2O^* \rightarrow H_2O_2 + OH$	(30)	
$OH + OH + M \rightarrow H_2O_2 + M$	(21)	$x10^{-17}(m^3s^{-1})$
$H + O_2 \rightarrow HO_2$	(53)	$x10^{-8}cm^3mol^{-2}s^{-1}$
$HO_2 + HO_2 \rightarrow H_2O_2 + O_2$	(31)	$x10^{-12}$ s^{-1}
$H + H_2O_2 \rightarrow H_2 + HO_2$	(27)	$x10^{-11}exp(-3162/Tg)$ (cm^3/s)
$OH + H_2O_2 \rightarrow H_2O + HO_2$	(11)	$x10^{10}$ $M^{-1}s^{-1}$
$O + H_2O_2 \rightarrow OH + HO_2$	(27)	$x10^{-12}exp(-1943.6/Tg)$
$OH + H_2O^* \rightarrow H_2 + HO_2$	(30)	-
Liquid phase		
$H_2O^+ + H_2O \rightarrow OH^- + H_3O^+$	(11,21,40)	$x10^{-15}m^3s^{-1}$
$H_3O^+ + HO_2^- \rightarrow H_2O_2 + H_2O$	(11)	$x10^{10}$ ($M^{-1}s^{-1}$)
$OH + OH^- \rightarrow H_2O + O^-$	(23)	$x10^{9}$ $M^{-1}s^{-1}$
$e^- + H_2O_2 \rightarrow OH^- + OH$	(17)	$11x10^{9}M^{-1}s^{-1}$
$H_2O_2 \rightarrow H_2O + 1/2\ O_2$	(14)	$2x10^{5}exp(-14800/RT)$

This preliminary reaction scheme is intended as a foundation for future modeling and simulation studies to elucidate the formation pathways of the observed species in this plasma configuration. In this sense, the reactions involving radical-radical interactions typically take place in the gas phase, but the reactions that involve high-energy plasma generated species (electrons, excited water, ionized argon) interacting with liquid water molecules, take place most likely in the plasma-liquid interface; and ultimately, the reactions involving ions (OH^-, H_3O^+, HO_2^-) interacting in solution, indicate they occur in the bulk liquid phase. OH ions are mostly formed in the liquid phase due to lower energy requirements for their life. Then, the classification of the reactions considered for our specific plasma-liquid system are collected in Table 1. An extension of table 1, including additional information about temperature and estimated enthalpy of formation, is presented in Supporting Information – Section 4.(54)

In general, reactions taking place in the gas phase are faster than in liquid phase, therefore for a simplified plug flow reactor model (PFR) we consider a constant supply of HP into the liquid phase. The model was fitted at specific conditions of pulse time (500 ns and 0.2 DC) and variation of power and residence time (Figure S15). The fitting shows that at input powers of 200, 300, 500 W the decomposition or the decay of HP is negligible and that higher residence time of the liquid in the plasma reaction zone would benefit the HP production, as it is also evident in Figure S15. On the contrary, at a power of 700 W the decay increases with residence time with a reaction rate constant of 0.04 s^{-1}. This is in line with the former discussion about the detrimental effect of higher temperatures and steam generation that occur at higher powers. Currently the system is limited to a minimum liquid flow rate of 0.2 mL/min, and in principle, allowing longer residence time of the liquid in the plasma zone would improve the HP production.

In this study, we demonstrated the feasibility of employing a conventionally considered warm plasma for the synthesis of the thermally sensitive HP. The strategy consisted of using a nanosecond pulsated microwave plasma, together with quenching, to enhance hydrogen peroxide production from water. A systematic test revealed tunable parameters, with pulsation frequency playing a key role (notably around 0.4 MHz). The species observed (like OH, and H Balmer lines) provided insights into the reaction steps. High-resolution, time-resolved studies helped us looking closer into how the process evolves along the microwave pulse. This technology represents a sustainable pathway for electrified HP production, with strong potential for on-site, on-demand applications. The maximum concentrations achieved in this work (ca. 0.17%) are similar to reported commercial concentrations (0.15%), (8) which is a safe range for on-site HP production using only water, electricity and argon in our case. As revealed by this work, a system capable of providing higher residence time for the liquid phase in the plasma zone would improve the production of HP.

ASSOCIATED CONTENT

Supporting Information

The supporting information is available free of charge on the ACS Publications website. Plasma-liquid reactor representation, plasma-liquid pictures, parameters and calculations, HR-OES analysis, calibration for HP concentration measurements, effect of plasma quenching, energy yield, production rate and gas to liquid ratio variation analysis, mass balance (PDF).

AUTHOR INFORMATION

Corresponding Author

Alexander Navarrete - *Institute for Micro Process Engineering, Karlsruhe Institute of Technology, Karlsruhe, 76344, Germany*. Email: alexander.navarrete@kit.edu

Authors

Mery Hernandez – *Institute for Micro Process Engineering, Karlsruhe Institute of Technology, Karlsruhe, 76344, Germany.*

Yannis Mikolaiczyk – *Institute for Micro Process Engineering, Karlsruhe Institute of Technology, Karlsruhe, 76344, Germany.*

Sergey Soldatov – *Institute for Pulsed Power and Microwave Technology, Karlsruhe Institute of Technology, Karlsruhe, 76344, Germany*

Guido Link - *Institute for Pulsed Power and Microwave Technology, Karlsruhe Institute of Technology, Karlsruhe, 76344, Germany*

Lucas Silberer – *Institute for Pulsed Power and Microwave Technology, Karlsruhe Institute of Technology, Karlsruhe, 76344, Germany*

Roland Dittmeyer – *Institute for Micro Process Engineering, Karlsruhe Institute of Technology, Karlsruhe, 76344, Germany.*

Notes

A patent application has been filed: A. Navarrete, R. Dittmeyer, M. Hernandez, Reactor for catalytic and chemical reactions facilitated by plasma environments, processes and uses (EP25180477,filed 03 June 2025).

ACKNOWLEDGMENT

The presented work was carried out within the framework of the Helmholtz program Materials and Technologies for the Energy Transition in the topic Chemical Energy Carriers and the subtopic Power-based Fuels and Chemicals. The authors acknowledge the funding support from the GreenSWaP project (ID: 101161583). Additionally, we are thankful with Prof. Peter Bruggeman for his feedback and support.

REFERENCES

(1) Seo, M. gi; Kim, H. J.; Han, S. S.; Lee, K. Y. Direct Synthesis of Hydrogen Peroxide from Hydrogen and Oxygen Using Tailored Pd Nanocatalysts: A Review of Recent Findings. *Catalysis Surveys from Asia*. Springer New York LLC March 2017. https://doi.org/10.1007/s10563-016-9221-y.

(2) Hargreaves, J. S. J.; Chung, Y. M.; Ahn, W. S.; Hisatomi, T.; Domen, K.; Kung, M. C.; Kung, H. H. Minimizing Energy Demand and Environmental Impact for Sustainable NH3 and H2O2 Production—A Perspective on Contributions from Thermal, Electro-, and Photo-Catalysis. *Applied Catalysis A: General*. Elsevier B.V. March 25, 2020. https://doi.org/10.1016/j.apcata.2020.117419.

(3) Gao, G.; Tian, Y.; Gong, X.; Pan, Z.; Yang, K.; Zong, B. Advances in the Production Technology of Hydrogen Peroxide. *Chinese Journal of Catalysis*. Science Press July 2020, pp 1039–1047. https://doi.org/10.1016/S1872-2067(20)63562-8.

(4) Goor, G.; Glenneberg, J.; Jacobi, S.; Dadabhoy, J.; Candido, E. Hydrogen Peroxide. In *Ullmann's Encyclopedia of Industrial Chemistry*; Wiley, 2019; pp 1–40. https://doi.org/10.1002/14356007.a13_443.pub3.

(5) Perry, S. C.; Mavrikis, S.; Wang, L.; Ponce de León, C. Future Perspectives for the Advancement of Electrochemical Hydrogen Peroxide Production. *Current Opinion in Electrochemistry*. Elsevier B.V. December 2021. https://doi.org/10.1016/j.coelec.2021.100792.

(6) *Universal Sustainable Development Goals*. https://sdgs.un.org/publications/universal-sustainable-development-goals-17850.

(7) Siahrostami, S. H2O2 Electrosynthesis and Emerging Applications, Challenges, and Opportunities: A Computational Perspective. *Chem Catalysis*. Cell Press March 2023. https://doi.org/10.1016/j.checat.2023.100568.

(8) *Products - HPNow*. https://hpnow.com/products/.

(9) Sun, Y.; Han, L.; Strasser, P. A Comparative Perspective of Electrochemical and Photochemical Approaches for Catalytic H2O2 production. *Chemical Society Reviews*. Royal Society of Chemistry September 21, 2020, pp 6605–6631. https://doi.org/10.1039/d0cs00458h.

(10) Lewis, R. J.; Hutchings, G. J. Recent Advances in the Direct Synthesis of H 2 O 2. *ChemCatChem*. Wiley Blackwell January 9, 2019, pp 298–308. https://doi.org/10.1002/cctc.201801435.

(11) Oinuma, G.; Nayak, G.; Du, Y.; Bruggeman, P. J. Controlled Plasma-Droplet Interactions: A Quantitative Study of OH Transfer in Plasma-Liquid Interaction. *Plasma Sources Sci. Technol.* **2020**, *29*. https://doi.org/10.1088/1361-6595/aba988.

(12) Hawtof, R.; Ghosh, S.; Guarr, E.; Xu, C.; Sankaran, R. M.; Renner, J. N. Catalyst-Free, Highly Selective Synthesis of Ammonia from Nitrogen and Water by a Plasma Electrolytic System. *Asian J. Chem.* **2019**, *31*. https://doi.org/10.1126/sciadv.aat5778.

(13) Cameli, F.; Dimitrakellis, P.; Chen, T. Y.; Vlachos, D. G. Modular Plasma Microreactor for Intensified Hydrogen Peroxide Production. *ACS Sustain. Chem. Eng.* **2022**, *10* (5), 1829–1838. https://doi.org/10.1021/acssuschemeng.1c06973.

(14) Lin, C. C.; Smith, F. R.; Ichikawa, N.; Baba, T.; Itow, M. Decomposition of Hydrogen Peroxide in Aqueous Solutions at Elevated Temperatures. *Int. J. Chem. Kinet.* **1991**, *23* (11), 971–987. https://doi.org/https://doi.org/10.1002/kin.550231103.

(15) Satterfield, C.; Stein, T. Decomposition of Hydrogen Peroxide Vapor on Relatively Inert Surfaces. *Ind. Eng. Chem.* **1957**, *49*, 1173–1180. https://doi.org/10.1021/ie50571a042.

(16) Du, Y.; Nayak, G.; Oinuma, G.; Peng, Z.; Bruggeman, P. J. Effect of Water Vapor on Plasma Morphology, OH and H2O2 Production in He and Ar Atmospheric Pressure Dielectric Barrier Discharges. *J. Phys. D. Appl. Phys.* **2017**, *50*. https://doi.org/10.1088/1361-6463/aa5e7d.

(17) Chen, Q.; Li, J.; Chen, Q.; Ostrikov, K. Recent Advances towards Aqueous Hydrogen Peroxide Formation in a Direct Current Plasma–Liquid System. *High Voltage*. John Wiley and Sons Inc June 1, 2022, pp 405–419. https://doi.org/10.1049/hve2.12189.

(18) Schüttler, S.; Schöne, A. L.; Jeß, E.; Gibson, A. R.; Golda, J. Production and Transport of Plasma-Generated Hydrogen Peroxide from Gas to Liquid. *Phys. Chem. Chem. Phys.* **2024**, *26*, 8255–8272. https://doi.org/10.1039/d3cp04290a.

(19) Chen, Z.; Cui, W.; He, Y. Mechanism of Hydrogen Peroxide Formation by Alternating Current and Direct Current Plasma Jets. *IEEE Trans. Plasma Sci.* **2022**, *50* (11), 4628–4635. https://doi.org/10.1109/TPS.2022.3211999.

(20) Liu, J.; He, B.; Chen, Q.; Li, J.; Xiong, Q.; Yue, G.; Zhang, X.; Yang, S.; Liu, H.; Liu, Q. H. Direct Synthesis of Hydrogen Peroxide from Plasma-Water Interactions. *Sci. Rep.* **2016**, *6*. https://doi.org/10.1038/srep38454.

(21) Bruggeman, P.; Schram, D. C. On OH Production in Water Containing Atmospheric Pressure Plasmas. *Plasma Sources Sci. Technol.* **2010**, *19* (4). https://doi.org/10.1088/0963-0252/19/4/045025.

(22) Tachibana, K.; Nakamura, T. Characterization of Dielectric Barrier Discharges with Water in Correlation to Productions of OH and H2O2 in Gas and Liquid Phases. *Jpn. J. Appl. Phys.* **2019**, *58* (4). https://doi.org/10.7567/1347-4065/aafe73.

(23) Lin, J.; He, X.; Chen, Q.; Xiong, Q.; Li, J.; Wang, X.; Chen, G.; Liu, Q. H.; Ostrikov, K. (Ken). The Formation Mechanism of Aqueous Hydrogen Peroxide in a Plasma-Liquid System with Liquid as the Anode. *Eur. Phys. J. D* **2020**, *74* (4). https://doi.org/10.1140/epjd/e2020-100371-2.

(24) Huang, S.; Liu, C.; Jie, Z.; Zhang, G. Imaging Diagnostics and Gas Temperature Measurements of Atmospheric-Microwave-Induced Air Plasma Torch. *IEEE Trans. Plasma Sci.* **2020**, *48* (6), 2153–2162. https://doi.org/10.1109/TPS.2020.2996017.

(25) Bogaerts, A.; Neyts, E. C. Plasma Technology: An Emerging Technology for Energy Storage. *ACS Energy Letters*. American Chemical Society April 13, 2018, pp 1013–1027. https://doi.org/10.1021/acsenergylett.8b00184.

(26) Hecimovic, A.; Mayer, M. T.; de Haart, L. G. J.; Gupta, S.; Kiefer, C. K.; Navarrete, A.; Schulz, A.; Fantz, U. Benchmarking Microwave-Induced CO2 Plasma Splitting against Electrochemical CO2 Reduction for a Comparison of Promising

Technologies. *J. CO2 Util.* **2024**, *83*. https://doi.org/10.1016/j.jcou.2024.102825.

(27) Vasko, C. A.; Liu, D. X.; Van Veldhuizen, E. M.; Iza, F.; Bruggeman, P. J. Hydrogen Peroxide Production in an Atmospheric Pressure RF Glow Discharge: Comparison of Models and Experiments. *Plasma Chem. Plasma Process.* **2014**, *34* (5), 1081–1099. https://doi.org/10.1007/s11090-014-9559-8.

(28) Liu, D. X.; Bruggeman, P.; Iza, F.; Rong, M. Z.; Kong, M. G. Global Model of Low-Temperature Atmospheric-Pressure He + H2O Plasmas. *Plasma Sources Sci. Technol.* **2010**, *19*. https://doi.org/10.1088/0963-0252/19/2/025018.

(29) Locke, B. R.; Shih, K. Y. Review of the Methods to Form Hydrogen Peroxide in Electrical Discharge Plasma with Liquid Water. *Plasma Sources Science and Technology*. June 2011. https://doi.org/10.1088/0963-0252/20/3/034006.

(30) Fridman, A. A. . *Plasma Chemistry*; Cambridge University Press. https://doi.org/https://assets.cambridge.org/97805218/47353/frontmatter/9780521847353_frontmatter.pdf.

(31) Chauvet, L.; Nenbangkaeo, C.; Grosse, K.; von Keudell, A. Chemistry in Nanosecond Plasmas in Water. *Plasma Process. Polym.* **2020**, *17* (6). https://doi.org/10.1002/ppap.201900192.

(32) Matsugi, A. Modeling Third-Body Effects in the Thermal Decomposition of H2O2. *Combust. Flame* **2021**, *225*, 444–452. https://doi.org/10.1016/j.combustflame.2020.11.019.

(33) Lamberts, T.; Samanta, P. K.; Köhn, A.; Kästner, J. Quantum Tunneling during Interstellar Surface-Catalyzed Formation of Water: The Reaction H + H2O2 → H2O + OH. *Phys. Chem. Chem. Phys.* **2016**, *18*, 33021–33030. https://doi.org/10.1039/C6CP06457D.

(34) Soldatov, S.; Link, G.; Silberer, L.; Schmedt, C. M.; Carbone, E.; D'Isa, F.; Jelonnek, J.; Dittmeyer, R.; Navarrete, A. Time-Resolved Optical Emission Spectroscopy Reveals Nonequilibrium Conditions for CO2Splitting in Atmospheric Plasma Sustained with Ultrafast Microwave Pulsation. *ACS Energy Lett.* **2021**, *6* (1), 124–130. https://doi.org/10.1021/acsenergylett.0c01983.

(35) Soldatov, S.; Carbone, E.; Kuhn, A.; Link, G.; Jelonnek, J.; Dittmeyer, R.; Navarrete, A. Efficiency of a Compact CO2 Coaxial Plasma Torch Driven by Ultrafast Microwave Power Pulsing: Stability and Plasma Gas Flow Dynamics. *J. CO2 Util.* **2022**, *58*. https://doi.org/10.1016/j.jcou.2022.101916.

(36) Wandell, R. J.; Locke, B. R. Hydrogen Peroxide Generation in Low Power Pulsed Water Spray Plasma Reactors. *Ind. Eng. Chem. Res.* **2014**, *53* (2), 609–618. https://doi.org/10.1021/ie402766t.

(37) Burlica, R.; Shih, K. Y.; Locke, B. R. Formation of H2and H2O2in a Water-Spray Gliding Arc Nonthermal Plasma Reactor. *Ind. Eng. Chem. Res.* **2010**, *49* (14), 6342–6349. https://doi.org/10.1021/ie100038g.

(38) Hsieh, K. C.; Wang, H.; Locke, B. R. Analysis of Electrical Discharge Plasma in a Gas-Liquid Flow Reactor Using Optical Emission Spectroscopy and the Formation of Hydrogen Peroxide. *Plasma Process. Polym.* **2016**, *13* (9), 908–917. https://doi.org/10.1002/ppap.201500204.

(39) Bruggeman, P.; Verreycken, T.; González, M. Á.; Walsh, J. L.; Kong, M. G.; Leys, C.; Schram, D. C. Optical Emission Spectroscopy as a Diagnostic for Plasmas in Liquids: Opportunities and Pitfalls. *J. Phys. D. Appl. Phys.* **2010**, *43* (12). https://doi.org/10.1088/0022-3727/43/12/124005.

(40) Lietz, A. M.; Kushner, M. J. Air Plasma Treatment of Liquid Covered Tissue: Long Timescale Chemistry. *J. Phys. D. Appl. Phys.* **2016**, *49*. https://doi.org/10.1088/0022-3727/49/42/425204.

(41) Qazi, H. I. A.; Nie, Q. Y.; Li, H. P.; Zhang, X. F.; Bao, C. Y. Comparison of Electrical and Optical Characteristics in Gas-Phase and Gas-Liquid Phase Discharges. *Phys. Plasmas* **2015**, *22* (12). https://doi.org/10.1063/1.4937779.

(42) Yusupov, M.; Neyts, E. C.; Simon, P.; Berdiyorov, G.; Snoeckx, R.; Van Duin, A. C. T.; Bogaerts, A. Reactive Molecular Dynamics Simulations of Oxygen Species in a Liquid Water Layer of Interest for Plasma Medicine. *J. Phys. D. Appl. Phys.* **2014**, *47*. https://doi.org/10.1088/0022-3727/47/2/025205.

(43) Bruggeman, P. J.; Kushner, M. J.; Locke, B. R.; Gardeniers, J. G. E.; Graham, W. G.; Graves, D. B.; Hofman-Caris, R. C. H. M.; Maric, D.; Reid, J. P.; Ceriani, E.; Fernandez Rivas, D.; Foster, J. E.; Garrick, S. C.; Gorbanev, Y.; Hamaguchi, S.; Iza, F.; Jablonowski, H.; Klimova, E.; Kolb, J.; Krcma, F.; Lukes, P.; MacHala, Z.; Marinov, I.; Mariotti, D.; Mededovic Thagard, S.; Minakata, D.; Neyts, E. C.; Pawlat, J.; Petrovic, Z. L.; Pflieger, R.; Reuter, S.; Schram, D. C.; Schröter, S.; Shiraiwa, M.; Tarabová, B.; Tsai, P. A.; Verlet, J. R. R.; Von Woedtke, T.; Wilson, K. R.; Yasui, K.; Zvereva, G. Plasma-Liquid Interactions: A Review and Roadmap. *Plasma Sources Science and Technology*. Institute of Physics Publishing September 30, 2016. https://doi.org/10.1088/0963-0252/25/5/053002.

(44) Gorbanev, Y.; O'Connell, D.; Chechik, V. Non-Thermal Plasma in Contact with Water: The Origin of Species. *Chem. - A Eur. J.* **2016**, *22*, 3496–3505. https://doi.org/10.1002/chem.201503771.

(45) Bruggeman, P.; Schram, D. C.; Kong, M. G.; Leys, C. Is the Rotational Temperature of OH(A-X) for Discharges in and in Contact with Liquids a Good Diagnostic for Determining the Gas Temperature? *Plasma Process. Polym.* **2009**, *6* (11), 751–762. https://doi.org/10.1002/ppap.200950014.

(46) Bruggeman, P.; Schram, D.; González, M. Á.; Rego, R.; Kong, M. G.; Leys, C. Characterization of a Direct Dc-Excited Discharge in Water by Optical Emission Spectroscopy. *Plasma Sources Sci. Technol.* **2009**, *18*. https://doi.org/10.1088/0963-0252/18/2/025017.

(47) Luo, Y.; Lietz, A. M.; Yatom, S.; Kushner, M. J.; Bruggeman, P. J. Plasma Kinetics in a Nanosecond Pulsed Filamentary Discharge Sustained in Ar-H 2 O and H 2 O. *J. Phys. D. Appl. Phys.* **2018**, *52*, aaeb14. https://doi.org/10.1088/1361-6463/aaeb14.

(48) Andrienko, D. A.; Boyd, I. D. Master Equation Study of Vibrational and Rotational Relaxations of Oxygen. *J. Thermophys. Heat Transf.* **2016**, *30*, 533–552. https://doi.org/10.2514/1.T4769.

(49) Brisset, A.; Gibson, A. R.; Schröter, S.; Niemi, K.; Booth, J. P.; Gans, T.; O'Connell, D.; Wagenaars, E. Chemical Kinetics and Density Measurements of OH in an Atmospheric Pressure He + O2+ H2O Radiofrequency Plasma. *J. Phys. D. Appl. Phys.* **2021**, *54*. https://doi.org/10.1088/1361-6463/abefec.

(50) Nikiforov, A. Y.; Leys, C.; Gonzalez, M. A.; Walsh, J. L. Electron Density Measurement in Atmospheric Pressure Plasma Jets: Stark Broadening of Hydrogenated and Non-Hydrogenated Lines. *Plasma Sources Sci. Technol.* **2015**, *24*. https://doi.org/10.1088/0963-0252/24/3/034001.

(51) Weiss, J. Radiochemistry of Aqueous Solutions. *Nature* **1944**, *153* (3894), 748–750. https://doi.org/10.1038/153748A0;KWRD=SCIENCE.

(52) Sun, H.; Li, Z. Rate Constant Measurement for the OH + OH → H 2O + O Reaction at 220-320 K Using Discharge Flow/Mass Spectrometer/Resonance Fluorescence Technique. *Chemical Physics Letters*. 2004, pp 33–38. https://doi.org/10.1016/j.cplett.2004.09.129.

(53) Elliot, A. J. Rate Constants And G-Values For The Simulation Of The Radiolysis Of Light Water Over The Range 0-300°C. *Atomic Energy of Canada Limited*. 1994, pp 1–69.

(54) Ruscic, B.; Pinzon, R. E.; Morton, M. L.; Von Laszevski, G.; Bittner, S. J.; Nijsure, S. G.; Amin, K. A.; Minkoff, M.; Wagner, A. F. *Introduction to active thermochemical tables: Several "Key" enthalpies of formation revisited*. Journal of Physical Chemistry A. https://doi.org/10.1021/jp047912y.